A Model-Based Technique with ℓ_1 Minimization for Defect Detection and RCS Interpolation from Limited Data

Ivan J. LaHaie, Steven M. Cossmann, and Michael A. Blischke

Integrity Applications, Inc. (IAI)
900 Victors Way, Suite 220, Ann Arbor, MI 48108
ilahaie@integrity-apps.com, scossmann@integrity-apps.com, mblischke@integrity-apps.com

Abstract ─ Method of moments (MoM) codes have become increasingly capable and accurate for predicting the radiation and scattering from structures with dimensions up to several tens of wavelengths. In an earlier work, we presented a network model (NM) algorithm that uses a Gauss-Newton iterative nonlinear estimation method in conjunction with a CARLOS-3D™ MoM model to estimate the "as-built" materials parameters of a target from a set of backscatter measurements. In this paper, we demonstrate how the NM algorithm, combined with the basis pursuits (BP) ℓ_1 minimization technique, can be used to locate unknown defects (dents, cracks, etc.) on a target from a limited set of RCS pattern measurements. The advantage of ℓ_1 minimization techniques such as BP is that they are capable of finding sparse solutions to underdetermined problems. As such, they reduce the requirement for a priori information regarding the location of the defects and do not require Nyquist sampling of the input pattern measurements. We will also show how the BP solutions can be used to interpolate RCS pattern data that is undersampled or has gaps.

Index Terms - ℓ_1 minimization, method of moments, RCS measurement.

I. INTRODUCTION

Recently, there has been an interest in the use of computational electromagnetics (CEM) prediction codes to improve the quality, efficiency, and utility of RCS measurements. This is especially true at lower frequencies (electrically small targets) where multiple interactions and narrow bandwidths limit the effectiveness of ISAR imaging for mitigation of measurement errors such as multipath and/or target support contamination or the detection of defects or changes on a target. Furthermore, these CEM-aided measurement techniques have applications beyond those of conventional imaging, including estimating the as-built values of surface impedances, near field-to-far field transformation, and interpolating RCS pattern data that is undersampled or has gaps.

Over the last several years, IAI staff have developed a specific implementation of a CEM-aided measurement technique known as the network model (NM) algorithm [1]. The NM algorithm is a model-based estimation technique that uses a full-wave method of moments (MoM) CEM code to predict the induced currents on the structure and associated radiated/scattered field patterns as part of the estimation process (although it can be extended in principle to other types of rigorous CEM codes). As such, the algorithm includes both single and multiple interactions and is applicable to both convex and concave shaped targets. The NM algorithm has been used in the past to mitigate illumination and multipath errors [2], [3] and to estimate the "as-built" equivalent surface impedance of non-PEC features and/or treatments of a target from a set of backscatter (RCS) measurements [4].

In this paper, which is an expansion of our 2012 AMTA Proceedings paper [5], we apply the NM algorithm to the problem of RF target diagnostics. Specifically, we demonstrate how the NM algorithm, combined with the basis pursuits (BP) ℓ_1 minimization technique, can be used to locate ***unknown*** defects (dents, cracks,

Submitted On: April 6, 2013
Accepted On: Aug. 27, 2013

etc.) on a target from a limited set of RCS pattern measurements. The advantage of ℓ_1 minimization techniques such as BP is that they are capable of finding sparse solutions to underdetermined problems. As such, they reduce the requirement for a priori information regarding the location and/or characteristics of the defects and do not require Nyquist sampling of the input pattern measurements. The fact that NM algorithm does not require specific knowledge or models of the defects makes it more generally applicable than methods where a "library" of one or more defect models is required (see, for example, the method described earlier in this journal [6]). We will also show how the BP solutions can be used to interpolate RCS pattern data that is undersampled or has gaps.

In Section II of this paper, we derive the iterative network model (NM) algorithm and briefly discuss its convergence properties. Section III provides numerical simulations of its performance for a simple canonical RCS shape using the CARLOS-3D™ MoM code [7]. The paper concludes with a summary and list of references in Sections 0 and V, respectively.

II. NETWORK MODEL ALGORITHM FORMULATION

The network model (NM) algorithm is a model-based technique for bringing a method-of-moments (MoM) scattering prediction into agreement with a corresponding set of measurements [1]-[5]. The formulation of the NM algorithm begins with the familiar matrix equation that arises in all MoM prediction codes [8], namely

$$\mathbf{Z}(\boldsymbol{\eta})\mathbf{j} = \mathbf{v}\,, \tag{1}$$

Here, $\mathbf{Z}$ is the target impedance matrix, written explicitly as a function of a vector of target model parameters $\boldsymbol{\eta}$, $\mathbf{j}$ is the vector of coefficients for the basis functions used to represent the induced (electric and magnetic) currents on the target, and $\mathbf{v}$ is the vector of excitation coefficients used to represent the incident field on the target. We will assume throughout that the incident field is a plane wave with a given polarization and direction of incidence (i.e., far-field illumination), but the derivation presented herein can be straightforwardly extended to arbitrary scattering and/or radiation measurements in the near or far field. Note that all of the quantities in Eq. (1) are implicit functions of frequency *f*.

Given the incident field and a model for the target geometry and its associated materials parameters, the MoM code computes $\mathbf{Z}$ and $\mathbf{v}$ and then solves Eq. (1) to find $\mathbf{j}$, viz.

$$\mathbf{j} = \mathbf{Z}^{-1}(\boldsymbol{\eta})\mathbf{v} = \mathbf{Y}(\boldsymbol{\eta})\mathbf{v}\,, \tag{2}$$

where $\mathbf{Y}$ is the MoM admittance matrix for the target.

Now consider a vector of measurements $\mathbf{s}$ and MoM predictions $\mathbf{s}_p$ of the target's far-field (FF) scattering pattern at set of M observation angles and polarizations. The units of $\mathbf{s}$ and $\mathbf{s}_p$ are defined such that the magnitude squared of any element is equal to the FF target RCS. From Eq. (2), the MoM prediction at the m^{th} observation angle and polarization can be written as

$$s_{pm}(\boldsymbol{\eta}) = \mathbf{r}_m^T\mathbf{j} = \mathbf{r}_m^T\mathbf{Y}(\boldsymbol{\eta})\mathbf{v}_m = \mathbf{r}_m^T\mathbf{Z}^{-1}(\boldsymbol{\eta})\mathbf{v}_m\,, \tag{3}$$

where $\mathbf{r}_m$ is a (known) radiation vector relating the induced current to the far-field scattering pattern, and T denotes the matrix transpose. In general, this is not the same as the m^{th} measurement s_m, even under error-free measurement conditions. This is because the MoM model for the target is never perfect. To that end, the vector $\boldsymbol{\eta}$ corresponds to a set of N parameters that are chosen to represent the sources of the differences between the target measurements and its MoM model predictions. For obvious reasons, we will refer to these as Z-parameters.

In its most general form, the network model seeks to estimate a set of N Z-parameters $\boldsymbol{\eta}$ that brings the MoM scattering predictions $\mathbf{s}_p$ into satisfactory agreement with the scattering measurements $\mathbf{s}$:

$$s_m \approx s_{pm}(\boldsymbol{\eta}) = \mathbf{r}_m^T\mathbf{Z}^{-1}(\boldsymbol{\eta})\mathbf{v}_m, \quad m = 1, \ldots, M\,, \tag{4}$$

subject to constraints on the allowable solutions $\boldsymbol{\eta}$. This is a (constrained) nonlinear system of M equations and N unknowns.

Inasmuch as it is reasonable to assume the initial MoM predictions are not grossly in error, a solution to Eq. (1) can be found using one of many standard gradient-based iterative techniques. In particular, we use a modified Gauss-Newton method, wherein at the k^{th} iteration, Eq. (1) is expanded in a first-order Taylor series about the current values $\boldsymbol{\eta}_{(k)}$ of the Z-parameters;

$$\mathbf{s} \approx \mathbf{s}_{p(k)} + \mathbf{G}_{(k)}\Delta\boldsymbol{\eta}_{(k)}, \quad (5)$$

where $\mathbf{s}_{p(k)} = \mathbf{s}_p\left(\boldsymbol{\eta}_{(k)}\right)$ are the current values of the MoM scattering predictions, and $\mathbf{G}_{(k)}$ is the Jacobian matrix whose elements are given by

$$G_{mn(k)} = \left.\frac{\partial s_{pm}}{\partial \eta_n}\right|_{\boldsymbol{\eta}=\boldsymbol{\eta}_{(k)}} = -\mathbf{r}_m^T\mathbf{Y}\left(\boldsymbol{\eta}_{(k)}\right)\mathbf{Q}_n\left(\boldsymbol{\eta}_{(k)}\right)\mathbf{Y}\left(\boldsymbol{\eta}_{(k)}\right)\mathbf{v}_m, \quad (6)$$

with

$$\mathbf{Q}_n(\boldsymbol{\eta}) = \frac{\partial \mathbf{Z}(\boldsymbol{\eta})}{\partial \eta_n}. \quad (7)$$

A solution $\Delta\boldsymbol{\eta}_{(k)}$ is then found that satisfies the linear system of equations (5) to within some acceptable value in a least squares sense, viz.

$$\left\|\Delta\mathbf{s}_{(k)} - \mathbf{G}_{(k)}\Delta\boldsymbol{\eta}_{(k)}\right\|_2 < \varepsilon_{(k)}, \quad (8)$$

subject to the constraints on the allowable solutions, where $\Delta\mathbf{s}_{(k)} = \mathbf{s} - \mathbf{s}_{p(k)}$. This is used to update the MoM model Z-parameters according to

$$\boldsymbol{\eta}_{(k+1)} = \mathsf{P}_C\left(\boldsymbol{\eta}_{(k)} + \beta\Delta\boldsymbol{\eta}_{(k)}\right), \quad (9)$$

where $0 < \beta \leq 1$ to control the step size of the update and P_C is a projection onto any constraints. The process is then repeated until acceptable agreement between the measurements $\mathbf{s}$ and predictions $\mathbf{s}_p$ is achieved.

In general, the performance of the NM algorithm will depend on the number of unknown Z-parameters N relative to the number of independent measurements M. This is evident in the fact that linear system in Eq. (5) consists of M equations and N unknowns. Historically, model-based estimation algorithms require $M > N$ for good performance, because in that case the resulting system of equations is well-posed and stable and can be solved using standard (e.g., least squares) techniques. Unfortunately, in many applications, the number of measurements M is either limited or we seek to reduce it. Similarly, in order to ensure that the NM algorithm is robust with respect to the how the "as-built" measured target and its numerical model differ, we want to work in situations where the number of Z-parameters N is large. This is because we don't want to assume that we know *a priori* where the discrepancies between the model and the target lie. It is therefore very likely that we will be faced with an underdetermined problem ($M < N$) whose solution is not just ill-posed, but in fact non-unique. In this case, it is necessary to impose constraints and/or conditions upon the allowable solution in order to stabilize ("regularize") the linear system solver.

Two common regularization methods involve minimizing, or at least bounding, the ℓ_2 or ℓ_1 norms of the solution. Each results in a solution with very different characteristics. For the underdetermined problem, ℓ_2 minimization solvers produce solutions that tend to be "spread out" across all of the unknowns. Conversely, ℓ_1 minimization solvers (such as BP) produce "sparse" updates where a smaller fraction of the unknowns are significant.

It follows that for the purposes of locating defects (cracks, gaps, dents, bumps) on a target, an ℓ_1 minimization solver may be the better choice because while the locations of the defects aren't known, it is likely that there will be a relatively small number of them. (Of course, it is always good to incorporate a priori information about possible defect locations if available in order to keep the number of Z-parameters required to model them at a minimum.) ℓ_1 minimization is also more likely to provide a more compact (better resolved) estimate of the defects' location, thereby helping to overcome the limited resolution typical of low frequency measurements.

We chose the MATLAB code SPGL1 [9] as the ℓ_1 minimization linear system solver for the NM algorithm. This code achieves ℓ_1 minimization by solving the basis pursuits (BP) denoising problem, which is characterized as

$$\min_{\Delta\boldsymbol{\eta}} \left\|\Delta\boldsymbol{\eta}\right\|_1 \quad s.t. \quad \left\|\Delta\mathbf{s} - \mathbf{G}\Delta\boldsymbol{\eta}\right\|_2 < \varepsilon, \quad (10)$$

where ε is the desired accuracy of the linear solution at each Gauss-Newton iteration (see Eq. (1)). In order to accomplish this, the SPGL1 code uses a recasting of Eq. (10) known as the LASSO problem, which is defined as

$$\min_{\Delta\boldsymbol{\eta}} \left\|\Delta\mathbf{s} - \mathbf{G}\Delta\boldsymbol{\eta}\right\|_2 \quad s.t. \quad \left\|\Delta\boldsymbol{\eta}\right\|_1 < \tau. \quad (11)$$

SPGL1 begins with a small τ (typically zero), and with repeated iterations determines a $\Delta\boldsymbol{\eta}$ which satisfies Eq. (11). If this solution does not satisfy Eq. (10), τ is increased and the iterations are repeated.

Note that these BP iterations form an inner loop inside the NM Gauss-Newton iterations. In the current NM implementation of the SPGLI

code, the BP loop is stopped at the current value of τ when Eq. (11) is satisfied without having to refine the value of $\Delta\boldsymbol{\eta}$.

III. NETWORK MODEL SIMULATIONS

Numerical simulations of the NM algorithm defect detection performance were conducted using the EMCC version of the CARLOS-3D™ MoM code [7]. The code was modified to provide the matrices and vectors required to implement the NM algorithm Gauss-Newton iterations.

The structure used in the simulations was a 20" version of the PEC NASA almond target [10]. Two versions of the almond were created: a pristine "showroom" version with no defects which was used as the initial model for the MoM predictions, and an "slightly used" version with four defects that was used as the source of the "measured" data. Two of the defects (bump and edge dent) were relatively small and the other two (gouge and large dent) were relatively large. Fig. 1 and Fig. 2 show the meshes used in the MoM simulations of the two versions of the almond.

Far-field backscatter data for both versions of the almond were generated using the CARLOS-3D™ code for all three polarizations ($\theta\theta$, $\phi\phi$, and $\theta\phi = \phi\theta$) along five 360° azimuth cuts in 1° increments about the almond at frequencies of 3, 3.5, 3.7, and 4 GHz. The cuts were at elevations ranging from $\theta = -20°$ to +20° in 10° increments, where 0° elevation is defined as the plane of symmetry intersecting the side of the almond.

Data from three of the "slightly used" almond target azimuth cuts ($\theta = -20°$, 0°, +20°) were provided to the NM as the "measured" data $\mathbf{s}$. The corresponding cuts for the "showroom" target were provided to the NM as the predicted data $\mathbf{s}_p$.

In order to model the defects without having to perturb the shape of the "showroom" almond target, each of its facets was allowed to have unknown impenetrable complex-valued surface impedance. These impedance values comprised a total of $N = 8000$ unknown Z-parameters $\boldsymbol{\eta}$ which the NM estimated in order to bring the MoM predictions into agreement with the measurements. While only an approximation to the true defects, this choice of Z-parameters allowed the derivatives $\mathbf{Q}$ in Eq. (7) to be computed efficiently and in closed form. The initial values of the Z-parameter facet impedances for the "showroom" target were taken to be zero Ohms/square (PEC).

The NM impedance estimates were used then to locate the defects and predict the backscatter data at the other two elevations ($\theta = -10°, +10°$).

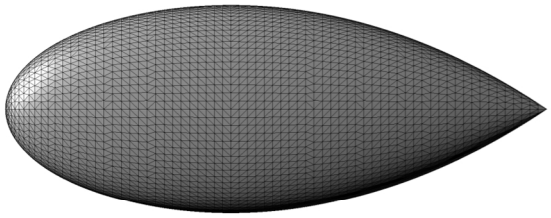

Fig. 1. MoM mesh for the "showroom" version of the 20" almond target (no defects).

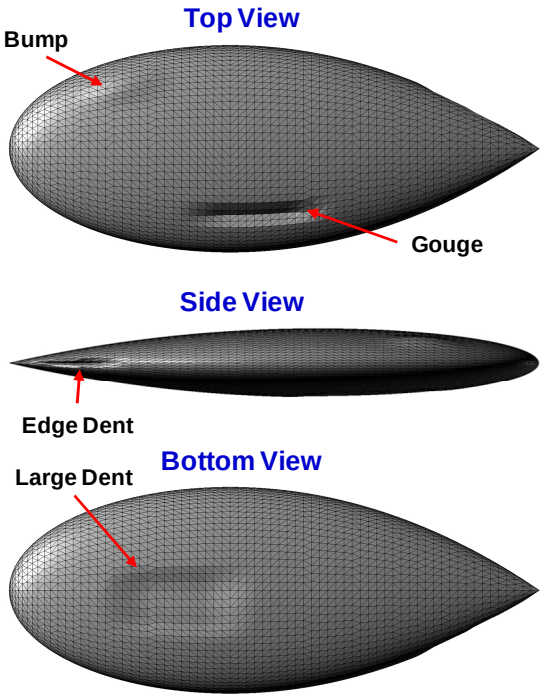

Fig. 2. MoM mesh for the "slightly used" version of the 20" almond target showing the four defects.

A. Single Frequency Defect Detection

Fig. 3 shows the absolute value of the estimated surface impedances found by the NM algorithm using the SPGL1 ℓ_1 minimization linear system solver using "measured" data at only a single frequency (4 GHz). The total number of independent measurements (based on Nyquist) for this case was $M = 255$. The estimates that differ substantially from zero (PEC) show a good correlation with the defect locations for the two

small defects (bump and edge dent). For the large dent defect, the NM estimates tend to correlate with its boundary rather than the entire extent of the defect. Finally, for the gouge defect, the non-zero NM impedance estimates correlate well with the defect location, but there are also a pair of additional "false alarm" artifacts adjacent to the gouge defect. These are likely due to the fact that we are using a surface impedance to approximate the defect, combined with using only single frequency data for the estimates.

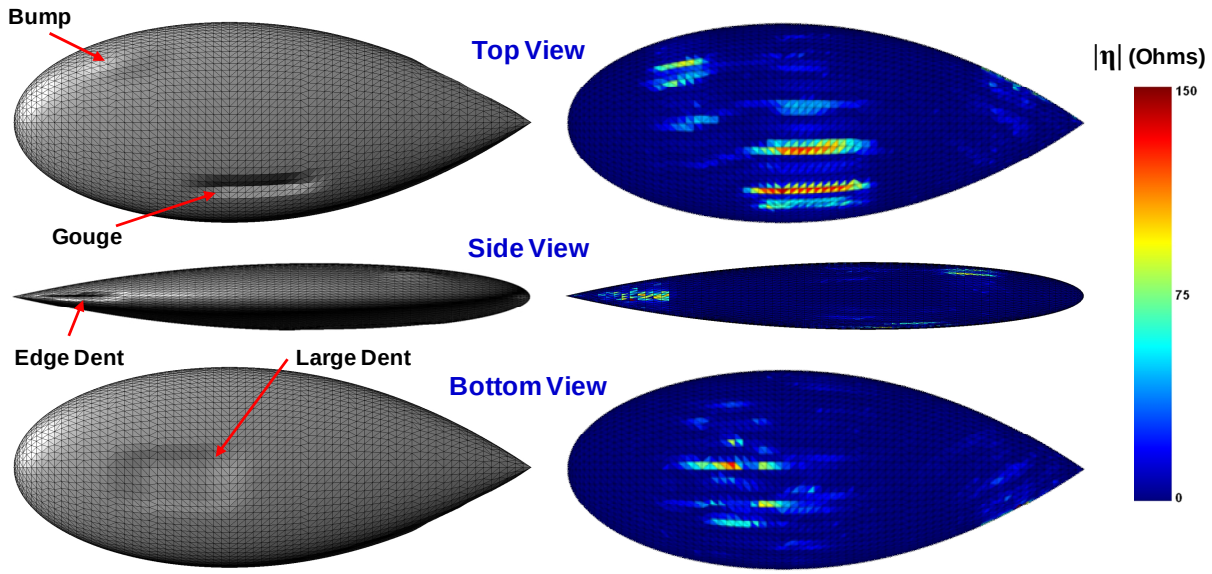

Fig. 3. Defects on the "slightly used" version of the almond target (left) compared to the BP single-frequency NM estimates of the facet surface impedances on the "showroom" version of the target (right).

Fig. 4 compares the NM estimates of the facet surface impedances obtained using the BP ℓ_1 minimization linear system solver to those obtained using a more traditional ℓ_2 minimization linear system solver, namely singular value decomposition (SVD). The estimates from each solver have been normalized to their respective peak values in order to better compare the two results. The figure clearly shows how ℓ_1 minimization results in a more sparse and localized estimate of the defect locations. It is worth noting the in both cases, the estimated impedances were almost purely reactive. This is not surprising because the defects do not contain any ohmic losses.

B. Multiple Frequency Defect Detection

In an attempt to reduce the "false alarm" artifacts in the NM impedance estimates, the results in Section III.A were repeated using the "measured" data at the other three frequencies (3.0, 3.5, and 3.7 GHz). The impedance estimates for all four frequencies were then averaged. The idea is that the false alarm artifacts will be uncorrelated with one another with sufficiently large changes in frequency.

Fig. 5 shows the absolute value of the averaged impedance estimates obtained from both the BP and SVD solvers. The results for each are shown on a scale that is normalized to the peak value of their respective averaged impedances. When compared to the 4 GHz single frequency estimates in Fig. 4, the results in Fig. 5 show that averaging the impedance estimates from multiple frequencies has reduced some of the artifacts, particularly for the SVD solver. That said, there remains a single, relatively large "false alarm" artifact associated with the gouge defect. In addition, frequency averaging does not appear to have substantially improved the detection of the large dent defect. It may be possible to improve the false alarm rejection by combining the multiple frequency results through some other method than averaging, such as M-out-of-N detection. Even better performance is potentially achievable by using all the frequencies jointly in the impedance estimation process.

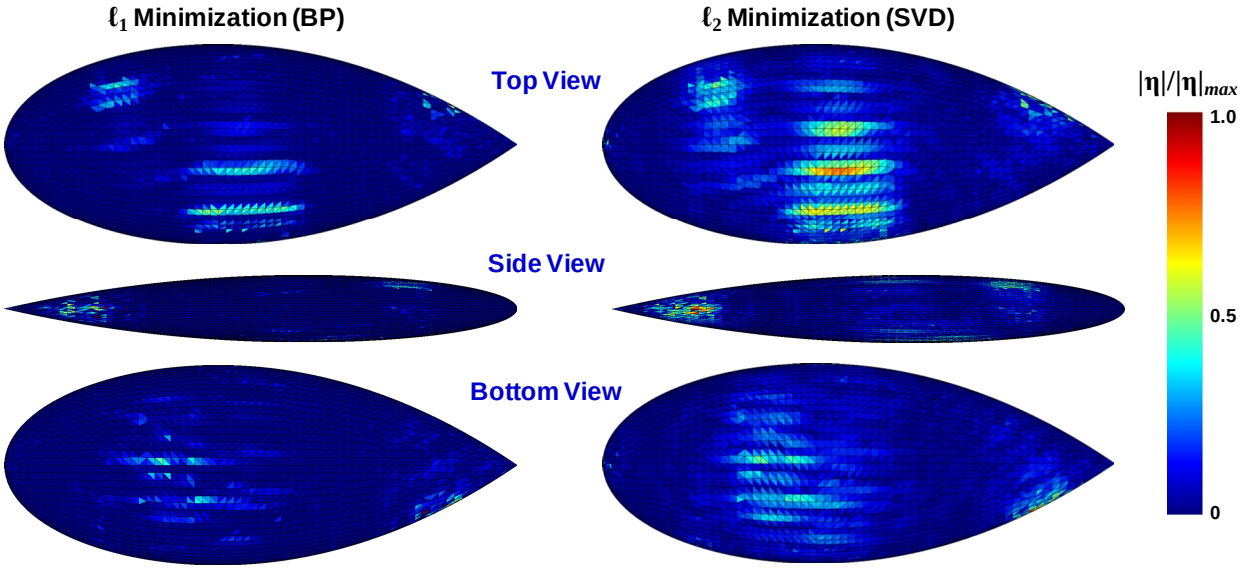

Fig. 4. Comparison of the BP (left) and SVD (right) single-frequency NM estimates of the facet surface impedances on the "showroom" version of the almond target. (Note that the images of the SVD results have been corrected from the original versions our AMTA paper [5].)

Fig. 5. Comparison of the BP (left) and SVD (right) frequency-averaged NM estimates of the facet surface impedances on the "showroom" version of the almond target.

C. Missing Data Interpolation

The single-frequency (4 GHz) NM impedance estimates were used to predict the RCS cuts of the "slightly used" target at the three "measured" and at two "unmeasured" elevation cuts. Plots of the mean RCS of the initial and final NM prediction error versus elevation angle for each of the five azimuth cuts are shown in Fig. 6, with the results from BP on the left and from SVD on the right. The prediction error is defined as the coherent difference between the "measured" data for the "slightly used" target and the MoM predictions for the "showroom" target.

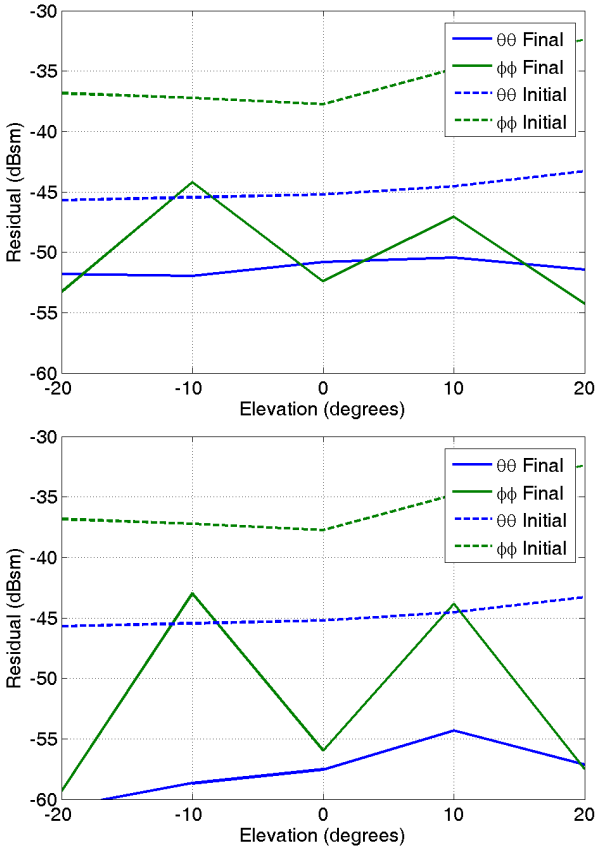

Fig. 6. Mean RCS versus elevation angle of the initial (dashed) and final (solid) NM prediction error obtained using the single-frequency (4 GHz) BP (top) and SVD (bottom) impedance estimates.

The plots show that the NM with BP solver has reduced the prediction error by 5-7 dB for θθ polarization and 15-20 dB for φφ polarization over the three azimuth cuts (θ = −20°, 0°, +20°) used to estimate the surface impedances. The corresponding reductions using the SVD solver are greater (10-15 dB for θθ polarization and 20-25 dB for φφ polarization). When one considers the two azimuth cuts (θ = −10°, +10°) that the were not part of the original "measured" data, the reductions are roughly the same as the measured cuts in θθ polarization over for both solvers. On the other hand, the reductions are less in φφ polarization, with BP performing 1-3 dB better than SVD.

IV. CONCLUSION

We have demonstrated the application of the iterative network model algorithm, combined with the basis pursuits (BP) ℓ_1 minimization technique, to the problem of locating unknown defects (dents, cracks, etc.) on a target from a limited set of RCS pattern measurements. The defects were modeled using an effective surface impedance. Numerical simulations of the NM algorithm performance were presented for the NASA almond target using the CARLOS-3D™ MoM code. The results showed that the use of a BP ℓ_1 minimization solver did a significantly better job of locating defects on the target relative to the more conventional ℓ_2 minimization (SVD) solver using data at a single frequency, although some artifacts were still present in the latter. Averaging the results from multiple frequencies further reduced the artifacts for both solvers. The results also showed that the estimated surface impedances could be used to accurately predict the target RCS at angles that were not part of the measured data.

As mentioned earlier, the approach described herein can be easily extended to include both near field and far field target measurements, so long as the near target illumination is known and can be modeled in the MoM code. An efficient technique for incorporating the illumination from an arbitrary antenna in MoM predictions is described in [11].

In future work, we plan on developing a parametric model for the frequency dependence of the defects that would allow us to use multiple frequencies jointly in the NM Gauss-Newton estimation algorithm. We expect this approach to work better for reducing false alarm artifacts relative to averaging the estimates obtain from applying the NM to each frequency individually.

V. REFERENCES

[1] J. F. Stach, "Numerical methods for measurement error mitigation," *Ant. Meas. Tech. Assoc. (AMTA) Proc.*, Williamsburg, VA, pp. 178-181, 1995.

[2] J. F. Stach, I. J. LaHaie, and E. I. LeBaron, "Multipath mitigation in compact RCS ranges using the network model and 2-D PML spectral estimation technique," *URSI North American Radio Science Meeting Dig.*, Montreal, CA, p. 731, 1997.

[3] J. F. Stach and J.W. Burns, "Mitigation of target illumination and multipath errors in ground plane RCS measurements," *Ant. Meas. Tech. Assoc. (AMTA) Proc.*, Montreal, Canada, pp. 67-71, 1998.

[4] C. M. Coleman, D. C. Love, M. A. Blischke, and I. J. LaHaie, "A technique for materials characterization from backscatter measurements," *Ant. Meas. Tech. Assoc. (AMTA) Proc.*, St. Louis, MO, pp. 116-121, 2007.

[5] I. J. LaHaie, S. M. Cossmann, and M. A. Blischke, "A model-based technique with ℓ_1 minimization for defect detection and RCS interpolation from limited data," *Ant. Meas. Tech. Assoc. (AMTA) Proc.*, Seattle, WA, pp. 139-144, 2012.

[6] F. Deek, M. El-Shenawee, "Microwave detection of cracks in buried pipes using the complex frequency technique," *Applied Computational Electromagnetics Society (ACES) Journal*, Vol. 25, No. 10, pp. 894-902, 2010.

[7] J. N. Putman and M. B. Gedera, "CARLOS-3D™: A general purpose three-dimensional method-of-moments scattering code," *IEEE Ant. Prop. Mag.*, Vol. 35, No. 2, pp. 69-71, 1993.

[8] R. F. Harrington, *Field Computations by Moment Methods*, Wiley-IEEE Press, New York, 1993.

[9] E. van den Berg and M. P. Friedlander, "Probing the Pareto frontier for basis pursuit solutions," *SIAM J on Scientific Computing*, Vol. 31, 0.2, pp. 890-912, 2008.

[10] A. C. Woo, et al., "Benchmark radar targets for the validation of computational electromagnetics programs," *IEEE Ant. Prop. Mag.*, Vol. 35, No. 1, pp. 84-89, 1993.

[11] I. J. LaHaie and M.A. Blischke, "Efficient Method for Representing Antenna Pattern Illumination in Method of Moments (MoM) Radar Cross-Section (RCS) Predictions," *Ant. Meas. Tech. Assoc. (AMTA) Proc.*, Denver, CO, pp. 41-45, 2011.

Ivan J. LaHaie received his BS degree in electrical engineering from Michigan State University in 1976, and his MS and Ph. D. degrees, also in electrical engineering, from the University of Michigan in 1977 and 1981, respectively. He joined the Environmental Research Institute of Michigan (ERIM) in 1980 and worked there for 30 years during its various incarnations as ERIM International, Veridian Systems, and General Dynamics Advanced Information Systems. He joined Integrity Applications Incorporated (IAI) in 2010, where he is currently a Principal Scientist in the Sensors and Analysis Sector. Dr. LaHaie's interests lie in the application of electromagnetics, inverse scattering, and signal processing techniques to problems in synthetic aperture radar (SAR) systems and phenomenology, unconventional RF and optical imaging, and radar cross-section (RCS) modeling, analysis, and measurements. Dr. LaHaie is a fellow of the Antenna Measurement Techniques Association (AMTA), a senior member of the Institute of Electrical and Electronics Engineers (IEEE), and a member of the Optical Society of America. He received the IEEE Aerospace and Electronic Systems Society Radar Systems Panel Award in 1991 and the AMTA Distinguished Achievement award in 2004.

Steven M. Cossmann received his BS and MS degrees in electrical engineering from Michigan State University in 2004 and 2006, respectively. He began working at General Dynamics Advanced Information Systems in 2006, and then moved to Integrity Applications Incorporated (IAI) in 2011, where he is currently a Systems Engineer in the Analytic Services Division. His primary interests are in applied and computational electromagnetics, radar cross-section (RCS) modeling and analysis, and inverse scattering.

Michael A. Blischke received his BS, MS, and Ph.D. in Electrical Engineering from Michigan State University in 1985, 1987, and 1989 respectively. He previously worked for Lockheed (later Lockheed Martin) beginning in 1989, and for ERIM International (later Veridian Systems, then General Dynamics Advanced Information Systems) beginning in 1998. He joined Integrity Applications Incorporated (IAI) in 2010, where he currently works performing design, analysis, and optimization in electromagnetics.